Research Square

Preprints are preliminary reports that have not undergone peer review.
They should not be considered conclusive, used to inform clinical practice,
or referenced by the media as validated information.

Climate Change Impacts on Reference Evapotranspiration in Arid and Semi-Arid Regions under CMIP6 Scenarios using ERA5-Land and Machine Learning

Ali Zolfaghari

azolfaghari@semnan.ac.ir

Semnan University

Maryam Raeesi

Semnan University

Giuseppe Longo-Minnolo

University of Catania Faculty of Agriculture: Universita degli Studi di Catania

Azade Soltani

Semnan University

Davoud Kartoulinezhad

Semnan University

Research Article

Keywords: CMIP6 Ensembles, ET0, Machine Learning, Reanalysis data, SSP Scenarios

Posted Date: July 7th, 2026

DOI: https://doi.org/10.21203/rs.3.rs-10125968/v1

License: This work is licensed under a Creative Commons Attribution 4.0 International License.
Read Full License

Climate Change Impacts on Reference Evapotranspiration in Arid and Semi-Arid Regions under CMIP6 Scenarios using ERA5-Land and Machine Learning

Ali Asghar Zolfaghari[1*], Maryam Raeesi[1], Giuseppe Longo-Minnolo[2], Azade Soltani[1], Davoud Kartoulinezhad[1]

1- Faculty of Desert Studies, Semnan University, Semnan, Iran

2- Department of Agriculture, Food and Environment (Di3A), University of Catania, Catania, Italy

***Corresponding Author: azolfaghari@semnan.ac.ir**

Abstract

Climate change significantly disrupts the hydrological cycle, particularly in arid and semi-arid regions like Semnan Province, Iran, which faces severe heat and water stress. This study evaluates the spatiotemporal impacts of future climate scenarios on reference evapotranspiration (ET_0) using the latest Coupled Model Intercomparison Project Phase 6 (CMIP6) climate ensembles. The research utilizes five CMIP6 models under the intermediate (SSP2-4.5) and high-emission (SSP5-8.5) Shared Socioeconomic Pathways across three time spans: near (2025–2050), mid (2051–2075), and far future (2076–2099). The methodology integrates the FAO Penman-Monteith equation with digital mapping, utilizing the Random Forest (RF) machine learning model to spatialize ET_0 at a 1 km resolution. To ensure local reliability, the ERA5-Land reanalysis data were downscaled from 9 km to 1 km using kriging and subsequently bias-corrected using Random Forest based on observed records from regional synoptic stations. GCM outputs were further downscaled via the Delta Change Factor (DCF) scaling method using the corrected ERA5-Land data as a reference. Sensitivity analysis confirmed that mean temperature is a dominant driver of ET_0 in this arid environment, with an annual sensitivity coefficient of 0.6. Results indicate steady warming across all horizons, with temperatures increasing by approximately 1°C per 30 years under SSP2-4.5 and 2°C per 30 years under SSP5-8.5. These thermal changes lead to projected ET_0 increases of 2.85 mm/year and 5.2 mm/year for the intermediate and high-emission scenarios, respectively. The analysis revealed that northern mountainous areas with denser vegetation cover are projected to experience more intense ET_0 increases compared to desert regions, suggesting a heightened vulnerability of agricultural zones to future moisture deficits. By the end of the century,

mean ET_0 is projected to rise by up to 16% relative to the baseline, necessitating adaptive water resource management and optimized irrigation to mitigate accelerating drought stress.

Keywords: CMIP6 Ensembles, ET_0, Machine Learning, Reanalysis data, SSP Scenarios

1. Introduction

Climate change is reshaping the global hydrological cycle through rising air temperatures, altered precipitation regimes, and more frequent extremes such as droughts and heatwaves, with particularly severe consequences in arid and semi-arid regions (IPCC, 2021; Jain and Singh, 2024). These changes directly influence water availability and agricultural sustainability by modifying atmospheric evaporative demand and evapotranspiration (ET), thereby affecting crop water requirements, irrigation scheduling, and water-resource planning (Disasa et al., 2025; Gou et al., 2020; Huang et al., 2022; Song et al., 2022; Wang et al., 2021).

Among ET-related indicators, reference evapotranspiration (ET_0) plays a central role as the standard climatic variable used to estimate crop evapotranspiration (ET_c) and irrigation water demand (Allen et al., 1998). ET_0 represents the evapotranspiration from a hypothetical, well-watered reference surface with uniform characteristics and therefore provides a consistent measure of atmospheric evaporative demand independent of crop type and management (Allen et al., 1998; Lai et al., 2022). In countries such as Iran, situated within the global arid and semi-arid belt and highly dependent on limited precipitation and groundwater, ET_0 constitutes a critical indicator for assessing climate-driven stress on agricultural water systems, where irrigation accounts for the dominant share of freshwater withdrawals (Karimi et al., 2024; Nasrollahi et al., 2021).

Recent studies indicate that climate change is likely to drive significant increases in ET_0 at both global and regional scales, largely driven by rising air temperatures (Hou et al., 2025). Increasing ET_0 intensifies soil moisture depletion, raises irrigation demand, and accelerates groundwater abstraction, thereby exacerbating drought risk and long-term water-security challenges (Cook et al., 2015; Frederick and Major, 1997). However, ET_0 responses to climate change are highly spatially heterogeneous and strongly dependent on emission scenarios, climate model structure, and downscaling techniques (Jerin et al., 2021; Yassen et al., 2020). In Iran, although several studies have projected future increases in temperature and ET_0, most rely on station-based observations, coarse-resolution climate datasets, or earlier-generation General Circulation Models (GCMs), limiting their capacity to capture local climatic gradients and spatial variability

(Cheshmberah and Zolfaghari, 2019; Heshmati and Sayari, 2021; Karimi et al., 2024; Mirhosseiny et al., 2021).

A major challenge in generating reliable ET_0 projections is the substantial uncertainty associated with future climate forcing. This uncertainty arises from inter-model variability among GCMs, emission pathways, bias-correction and downscaling procedures, and the sensitivity of ET_0 formulations to multiple climatic inputs such as wind speed, humidity, and radiation (Lai et al., 2022; Vanella et al., 2022; Ippolito et al., 2024). In this context, approaches that prioritize temperature, the most consistently projected and physically dominant driver of evaporative demand, offer a robust and pragmatic basis for first-order regional ET_0 assessments, particularly in data-scarce regions characterized by complex topography and sparse meteorological networks.

In recent years, increasing attention has been given to combining physically based climate projections with data-driven methods to enhance the spatial representation of hydroclimatic variables. Machine learning techniques, in particular, have shown strong potential for downscaling and bias correction of reanalysis and climate model outputs by capturing complex, nonlinear relationships between large-scale atmospheric drivers and local climatic responses (Najafi et al. 2026). Such hybrid frameworks provide an effective means of bridging the gap between coarse-resolution climate information and the fine-scale data needs of water-resource management, especially in regions where observational networks are sparse or unevenly distributed. Integrating CMIP6 ensembles with reanalysis products and machine-learning-based spatialization therefore represents a promising and increasingly adopted strategy for producing actionable, high-resolution assessments of climatic evaporative demand.

Semnan Province, located along the transition between the Alborz Mountains and the central deserts of Iran, exhibits pronounced climatic gradients and high vulnerability to heat and water stress. The region encompasses diverse agro-climatic zones and relies heavily on groundwater-based irrigation, making it especially sensitive to climate-driven changes in evaporative demand. These characteristics make Semnan Province a suitable case study for spatially explicit ET_0 analysis at fine resolution.

Accordingly, this study aims to (i) project future changes in ET_0 across an arid and semi-arid region in central Iran using an ensemble of five CMIP6 models under the intermediate (SSP2-4.5) and high-emission (SSP5-8.5) scenarios; (ii) integrate ERA5-Land reanalysis data with a Random Forest (RF) framework for high-resolution (1 km) bias correction and spatial downscaling; and

(iii) quantify spatiotemporal trends in temperature and ET_0 to support climate-adaptive water management and irrigation planning in this water-stressed arid region.

2. Materials and Methods

2.1 Study Area

Semnan Province is located on the southern slopes of the Alborz mountain range, with elevations decreasing from north to south (Heravi and Zolfaghari 2024). Situated in the central part of Iran, the province covers an area of approximately 97,491 km² (about 5.9% of the country's total land area) and extends from 34°15′ to 37°20′ N latitude and from 51°50′ to 57°03′ E longitude. The region is characterized by an arid to semi-arid climate, with low precipitation and high evapotranspiration, particularly in the southern areas. The mean annual temperature, precipitation, and reference evapotranspiration (ET_0) are approximately 18.5 °C, 138 mm, and 2,500 mm yr^{-1}, respectively (Raeesi et al. 2019). Large portions of the province, especially from the central to southern zones, are influenced by surrounding deserts and salt flats. Climatic conditions exhibit strong spatial heterogeneity, with precipitation decreasing sharply from more than 350 mm in the northern mountainous regions to less than 100 mm in the southern Dasht-e Kavir, accompanied by a concurrent increase in air temperature along the same gradient. Figure 1 shows the geographical location of Semnan Province in Iran.

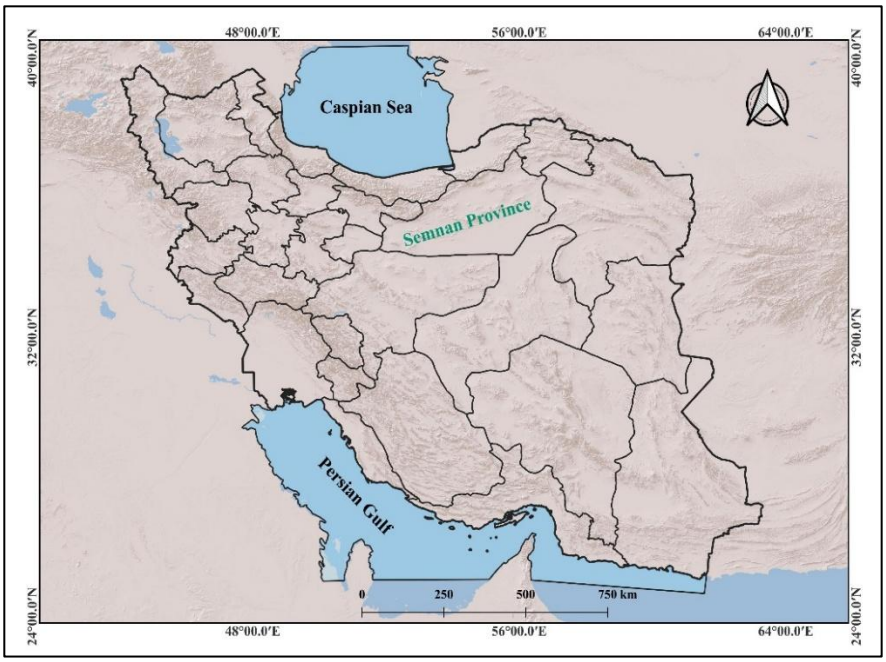


Figure_1 Geographical Setting of the Study Area

2.2 Reference Evapotranspiration using the FAO Penman-Monteith Method

In this study, the estimation of ET_0 was conducted through a two-stage workflow designed to ensure both physical consistency and high-resolution spatial representation. Stage 1 aimed to establish a reliable baseline and sensitivity reference by computing station-based daily ET_0 using the FAO-56 Penman–Monteith method, as recommended by the Food and Agriculture Organization (Allen et al., 1998). For this purpose, daily ET_0 was calculated at synoptic stations using a custom implementation of the FAO-56 algorithm (Nasrollahi et al., 2021). Daily meteorological variables, including maximum and minimum air temperature, relative humidity, wind speed, and solar radiation, were available for all stations and imported separately for each site. Standard quality control procedures were applied to check for missing or erroneous values, and only days with complete meteorological records were retained for ET_0 computation. The standardized FAO-56 computational procedure was then applied to generate daily ET_0 values, which were subsequently aggregated to derive annual ET_0 values using Equation (1).

Stage 2 focused on the spatialization of annual ET_0 at high resolution (1 km) using a Random Forest (RF) machine-learning framework. The target variable used to train the RF model was station-based annual ET_0, aggregated from daily FAO-56 estimates obtained in Stage 1. As predictors, gridded air temperature and ET_0 products from the ERA5-Land reanalysis dataset (original spatial resolution of 0.1° and daily temporal resolution) were used, together with a digital elevation model (DEM) at 30 m resolution, which was resampled to 1 km to match the target grid (Heravi and Zolfaghari 2024). The RF model was trained using data from the baseline period (1990–2014), using observations from 10 stations and a total of 240 training samples, and the trained model was subsequently applied to generate continuous gridded ET_0 surfaces across Semnan Province at 1 km resolution, enabling the representation of fine-scale spatial variability and providing spatially explicit ET_0 fields for subsequent trend analysis and future climate projections. The FAO-56 Penman–Monteith equation for ET_0 is as follow:

$$ET_0 = \frac{0.408\Delta(R_n - G) + \gamma \frac{900}{T+273} u_{2(e_s - e_a)}}{\Delta + \gamma(1 + 0.34u_2)} \qquad \textbf{Equation (1)}$$

where ET_0 is the reference evapotranspiration (mm day^{-1}), R_n is the net radiation at the crop surface (MJ m^{-2} day^{-1}), G is the soil heat flux density (MJ m^{-2} day^{-1}), T is the mean daily air temperature

at 2 m height (°C), U_2 is the wind speed at 2 m height (m s^{-1}), e_s is the saturation vapor pressure (kPa), e_a is the actual vapor pressure (kPa), (e_s - e_a) is the saturation vapor pressure deficit (kPa), Δ is the slope of the saturation vapor pressure curve (kPa $°C^{-1}$), and γ is the psychrometric constant (kPa $°C^{-1}$).

2.3 Sensitivity Analysis for Future Reference Evapotranspiration Estimates

In multivariate models such as the FAO Penman-Monteith equation, where variables have different dimensions and ranges of variation, the use of partial derivatives for sensitivity analysis is challenging. Under these conditions, partial derivatives must be transformed into dimensionless parameters to facilitate comparisons among climatic variables. Therefore, in the present study, sensitivity analysis of the climatic parameters in the FAO Penman-Monteith model was performed using Equation (2) (Beven 1979).

$$Sv_i = \frac{\partial ET_0}{\partial V_i} \cdot \frac{V_i}{ET_0} \qquad \textbf{Equation (2)}$$

where v_i represents the climatic variables (including T_{max} and T_{min} separately), and S_{v_i} is the dimensionless sensitivity coefficient for variable v_i. In essence, S_{v_i} indicates the percentage change in ET_0 resulting from changes in the climatic variables; a positive $S_{v_i} > 0$ implies that ET_0 and v_i increase concurrently. Additionally, a sensitivity coefficient of 0.1 for a variable indicates a 1% increase in ET_0 if the variable increases by 10%.

The FAO Penman–Monteith model incorporates multiple climatic variables, including minimum and maximum air temperature, relative humidity, and wind speed. In this study, temperature was identified as the dominant driver of ET_0 variability, consistent with previous findings in arid and semi-arid regions. Accordingly, future ET_0 variations were projected by focusing on thermal forcing, under the assumption that the relative contributions of humidity and wind speed remain secondary compared to the dominant temperature trend in these environments. Given the high uncertainty and inter-model variability associated with GCM projections of wind speed and relative humidity, their inclusion would introduce substantial noise into the regional assessment. This approach therefore provides a temperature-driven estimate of ET_0 change and represents a first-order approximation, which may under- or overestimate future ET_0 responses in regions where changes in humidity or wind speed are substantial.

To estimate temperature sensitivity, random simulated daily minimum and maximum temperature values were generated 1,000 times within the observed range of each variable for each day, while all other FAO-56 input variables were held constant. The FAO Penman–Monteith model was then executed using these perturbed temperature inputs to calculate daily sensitivity coefficients, following the procedure described by Nasrollahi et al. (2021). The resulting daily coefficients were subsequently averaged to derive monthly, seasonal, and annual sensitivity values.

2.4 Baseline Annual Temperature Variability and Digital Map Development

Accurate estimation of future annual ET_0 requires an assessment of the impacts of climate change and projections of the key influencing variable, namely temperature. Most climate change studies project climatic variables at locations where measurements are available (e.g., synoptic, climatological, or rain gauge stations), with fewer investigations addressing spatial variations at the provincial or watershed scale. However, stations capable of providing the data necessary for ET_0 estimation are limited in number and often distant from many agricultural and natural lands, potentially leading to errors in those areas.

In this study, ET_0 and temperature were estimated for each pixel across the entire study area. The workflow for developing baseline and future temperature maps involved the following sequence: (i) downscaling ERA5-Land data to 1 km resolution, (ii) bias-correcting the downscaled ERA5-Land data using station observations via a Random Forest (RF) model, (iii) using the bias-corrected ERA5-Land data as a gridded reference to validate and bias-correct CMIP6 model outputs, and (iv) creating baseline (1990–2014) and future (2015–2100) temperature maps at 1 km resolution. To estimate temperature at each pixel for the baseline period 1990–2014 (selected to align with the CMIP6 historical simulation period for consistent model validation and bias correction), temperature data from ERA5-Land were utilized; ERA5-Land data for 2015–2020 were additionally included for supplementary validation of the bias-correction process but not for the primary baseline maps. Initially, ERA5-Land data for Semnan Province were downloaded at a resolution of 9 km, after which these data were downscaled to a 1 km resolution using ordinary kriging. This method incorporated elevation as an external drift variable (to account for its strong influence on temperature variations), a spherical variogram model fitted to the empirical variogram, and leave-one-out cross-validation to assess performance.

ERA5-Land data are typically associated with biases; therefore, correction using station observations is necessary. In this study, the downscaled ERA5-Land data were bias-corrected

using measurements from synoptic and climatological stations, employing RF model for debiasing. Specifically, the RF model was trained using station-observed temperatures as the response variable and the following predictors: downscaled ERA5-Land temperature at corresponding station locations, elevation, and geographic coordinates (latitude and longitude). The RF model was validated using leave-one-station-out cross-validation and train/test data splitting. The model was fitted using data from station points and then applied to predict corrections across the entire gridded ERA5-Land dataset. For validation, a leave-one-station-out cross-validation approach was used. The corrected data were then used as a bias-corrected gridded reference dataset (as a gridded observational reference) and employed for validating climate change models and bias-correcting CMIP6 model outputs in future periods.

Numerous studies have demonstrated that ensembles of multiple models provide a superior approach compared to reliance on a single climate model for projecting climatic variables, as uncertainties, particularly in long-term projections, are better captured and represented in ensembles. Accordingly, in this study, five General Circulation Models (GCMs) were selected for projecting temperature in arid and semi-arid regions, based on which annual temperature projections were generated. These data were downloaded from the official ESGF website. The selection of these CMIP6 models was based on the availability of temperature data for both historical simulations (1990–2014) and projected scenarios (2015–2099).

As GCMs produce outputs at the global scale with large grid cells (Table 1), they may lead to over- or underestimation of climatic variables at the regional scale and fail to capture variations at finer resolutions (Ahmadalipour et al. 2017; Raeesi et al. 2024).

Table 1. Climate models used for future projections of air temperature (2 meters above ground level)

Climate Model	Providing Country	Native grid resolution	Nominal Spatial Resolution	Time Scale
ACCESS-CM2	Australia	1.25º×1.87º	250 km	Monthly
BCC-CSM2-MR	China	1.1º×1.1º	100 km	Monthly
CAMS-CSM1-0	China	1.1º×1.1º	100 km	Monthly
MIROC6	Japan	1.4º×1.6º	250 km	Monthly
Tai_ESM1	Taiwan	0.9º×1.25º	~100 km**	Monthly

**Note: The nominal spatial resolution for the TaiESM1 model is approximated to 100 km, based on the 0.9° × 1.25° grid spacing (equivalent to approximately 100 km × 139 km at the equator), following standard conventions in CMIP6 model documentation for summarizing horizontal resolution.

To project annual temperature scenarios for Semnan Province under future climate conditions, outputs from Coupled Model Intercomparison Project Phase 6 (CMIP6) General Circulation Models/Earth System Models (GCMs/ESMs) were utilized. These outputs were based on the

updated Shared Socioeconomic Pathways (SSPs), specifically the intermediate scenario (SSP2-4.5) and the very high-emission (pessimistic) scenario (SSP5-8.5), as outlined in the Sixth Assessment Report (AR6) of the Intergovernmental Panel on Climate Change (IPCC) for projecting climatic variables such as precipitation and temperature. The various SSP scenarios employed in CMIP6 project global socioeconomic changes up to the end of the 21st century (i.e., 2099).

2.5 Data Preparation and Preprocessing

To employ climate model outputs for future projections, it is essential to evaluate the simulated data from each model and validate them against ground-based observational data with appropriate spatial coverage to quantify model uncertainties (Alaminie et al. 2021). Climate models are available at the global scale and are therefore coarse-resolution; their outputs are generally unsuitable for regional studies, as they may cover the study area with only a few pixels exhibiting relatively uniform temperature values, leading to substantial errors.

Thus, a method must be selected to refine the spatial resolution of the data to better align with the study area (at regional or local scales) while correcting associated biases. In this study, maps from all climate models for the period 1990–2099 were initially resampled to a 1,000 m cell size using bilinear interpolation as a grid-matching step to align with the resolution of the downscaled ERA5-Land data; this resampling does not add new spatial information or constitute true statistical or dynamical downscaling but rather prepares the data for subsequent bias correction, with physical variability at finer scales introduced through the bias-corrected ERA5-Land reference dataset and the overall bias-correction framework. At this stage, the bias-corrected temperature maps from ERA5-Land served as a gridded reference for debiasing the climate model outputs through the end of the 21st century.

After regridding CMIP6 outputs to the 1 km reference grid and using the bias-corrected ERA5-Land data as a gridded reference, bias correction was applied on a per-cell basis. All processing related to bias correction of temperature outputs from CMIP6 models, based on the gridded reference during the historical calibration period (1990–2014), was performed in the R Studio environment (version 2021.09.1), utilizing key packages such as raster for spatial data handling, rgdal for geospatial data abstraction, and Metrics for goodness-of-fit evaluation. Future projection periods for the temperature variable were divided into three time horizons: near-future (2025–2050), mid-future (2051–2075), and far-future (2076–2099). Additionally, to reduce uncertainty

associated with individual models, an equal-weight arithmetic mean ensemble was computed after bias correction across the five model projections and used for temperature forecasting.

2.6 Bias Correction of Climate Model Outputs Using the Scaling Method

To correct biases in climate model outputs, the annual mean temperature values from the historical simulations of each model (simulated values) were compared on a per-cell basis with those from the corresponding observational time series (downscaled and bias-corrected ERA5-Land) to determine the discrepancy between the two datasets. Bias correction was then performed using the Delta Change Factor (DCF) method (Equations 3 and 4).

In essence, to obtain the error correction factor for climate model outputs, the observational values were divided by the historical values (1990–2014), yielding a scaling factor. This factor was subsequently multiplied by the pixel values of the future projections (2015–2100) to correct the model outputs for temperature.

$$T_{contr}^{BC}(\mathrm{t}) = T_{obs}(t) \qquad \textbf{Equation (3)}$$

$$T_{frc}^{BC}(\mathrm{t}) = T_{obs}(t).\left[\frac{\mu_m T_{frc}(t)}{\mu_m T_{contr}(t)}\right] \qquad \textbf{Equation (4)}$$

In the aforementioned equations, T represents temperature, contr denotes the number of simulated GCM series during the control period, obs refers to the observational time period, and frc indicates the future projected time series requiring bias correction. BC represents the bias-corrected future projected time series. Here, t denotes the time step, and μm is the long-term annual mean, which was subsequently aggregated to annual means after bias correction.

Ultimately, considering the uncertainties associated with the models ,bias correction was applied to the monthly temperature outputs for each individual CMIP6 model under the SSP2-4.5 and SSP5-8.5 scenarios; following this, monthly values were aggregated to annual means, and then the ensemble mean was computed across the bias-corrected models. The resulting ensemble projections were divided into three future time horizons: near-future (2025–2050), mid-future (2051–2075), and far-future (2076–2099). The ensemble mean under each scenario was extracted separately for the aforementioned time periods.

2.7 Model Performance Evaluation

Evaluating the accuracy and performance of models constitutes a fundamental step in the modeling process. In the present study, various statistical metrics were employed to assess model

performance, including the coefficient of determination (R^2), root mean square error (RMSE), bias (Bias), Pearson correlation coefficient (r), and root relative squared error (RRSE). The equations corresponding to each statistical metric are provided below (Equations 5–9).

$$R^2 = 1 - \frac{\sum_{i=1}^{n}(O_i - P_i)^2}{\sum_{i=1}^{n}(O_i - \bar{O})^2} \quad \textbf{Equation (5)}$$

$$RMSE = \sqrt{\frac{\sum_{i=1}^{n}(P_i - O_i)^2}{n}} \quad \textbf{Equation (6)}$$

$$Bias = \frac{1}{n}\sum_{i=1}^{n}(P_i - O_i) \quad \textbf{Equation (7)}$$

$$r = \frac{\sum_{i=1}^{n}(O_i - \bar{O})(P_i - \bar{P})}{\sqrt{\sum_{i=1}^{n}(O_i - \bar{O})^2}\sqrt{\sum_{i=1}^{n}(P_i - \bar{P})^2}} \quad \textbf{Equation (8)}$$

$$MAE = \frac{|O_i - P_i|}{n} \quad \textbf{Equation (9)}$$

In these equations, which were used to evaluate the performance of the RF model for debiasing ERA5-Land temperature data against station observations, the RF model for spatializing ET_0 against station measurements, and the bias-correction of CMIP6 model outputs validated against the gridded reference for the hold-out period 2015–2020, P_i and O_i represent the predicted and observed values, respectively; n is the number of data points; and $\bar{O}$ denotes the mean of the observed values. The RMSE is always positive, with values closer to zero indicating higher model accuracy. A positive Bias signifies overestimation, while a negative value indicates underestimation; a Bias close to zero reflects appropriate predictive accuracy. A correlation coefficient close to 1 denotes strong positive correlation, close to –1 indicates strong negative correlation, and values near zero suggest weak correlation between observed and predicted data. Furthermore, lower RRSE values indicate superior predictive performance relative to the baseline model, with a value of 1 signifying equivalent performance.

3. Results

3.1 Bias Correction of ERA5-Land Temperature Data for the Study Area

Table 2 presents the results of bias correction applied to the ERA5-Land temperature data in the study area. The findings indicate that the RMSE of the temperature values before bias correction was 2.35 °C annually, which decreased to 1.00 °C after bias correction. Additionally, the bias values between the station observations and the ERA5-Land reanalysis data decreased from 1.70 °C to -0.01 °C, indicating a substantial reduction of systematic error to near-zero levels. The r values between observed and reanalysis data before bias correction decreased from 0.84 ($p < 0.001$) before correction to 0.94 ($p < 0.001$) after correction. The MAE for annual temperature data prior to bias correction was approximately 1.81 °C, which reduced to 0.77 °C following bias correction (Table 2).

Table 2. Statistical metrics calculated before and after bias correction of ERA5-Land temperature data using the Random Forest (RF) method

Statistic	RMSE (°C)	Bias (°C)	r	R^2	MAE (°C)
Before bias correction	2.35	1.70	0.84^{**}	0.71^{**}	1.81
After bias correction	1.00	-0.01	0.94^{**}	0.89^{**}	0.77

** indicates significant differences at $p < 0.01$.

Figure 2 illustrates the scatter plots of observed temperature data versus ERA5-Land reanalysis temperature data before and after bias correction, with the 1:1 line included, for synoptic and climatological stations in the study area. The scatter plots reveal that the original ERA5-Land data exhibit systematic bias (positive bias of 1.70°C), overestimating temperature values compared to ground observations. In contrast, the results demonstrate that the RF machine learning method effectively corrected the annual temperature data based on observed records in Semnan Province, substantially reducing systematic errors in the ERA5-Land reanalysis data, and improving the accuracy of annual temperature estimates in the study area. The RF bias correction was validated using leave-one-station-out cross-validation to ensure robustness and generalizability across independent stations**.** These findings also indicate that, given the high accuracy of the bias-corrected ERA5-Land data, they can be reliably used as a gridded observational reference, following validation against station measurements.

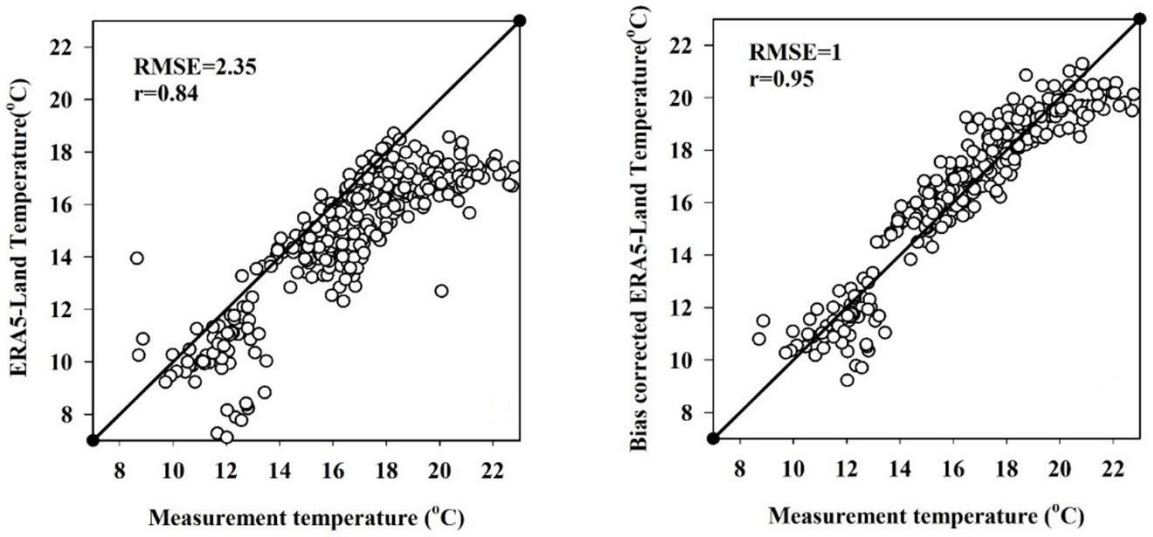


Figure_2 Scatter plots of temperature changes before (left) and after (right) bias correction, with the 1:1 line included, for synoptic and climatological stations in the study area

The spatial distribution of downscaled and bias-corrected ERA5-Land data for the study area is illustrated in Figure 3. The results demonstrate pronounced spatial variability across Semnan Province, with mean annual temperatures ranging from a minimum of 8.62 °C in the northern mountainous regions to a maximum of 22.83 °C in the southern arid zones. The median annual temperature was determined to be approximately 20.5 °C, signifying that half of the province's spatial extent experiences mean temperatures below this threshold, while the remaining half exceeds it. This temperature gradient is fundamentally driven by the regional topography; as elevation descends from the southern slopes of the Alborz mountain range in the north toward the central deserts and salt flats in the south, a systematic increase in temperature is observed. Consequently, the highest temperatures are concentrated in the central and southern parts of the province, reflecting the transition toward low-elevation arid and desert environments.

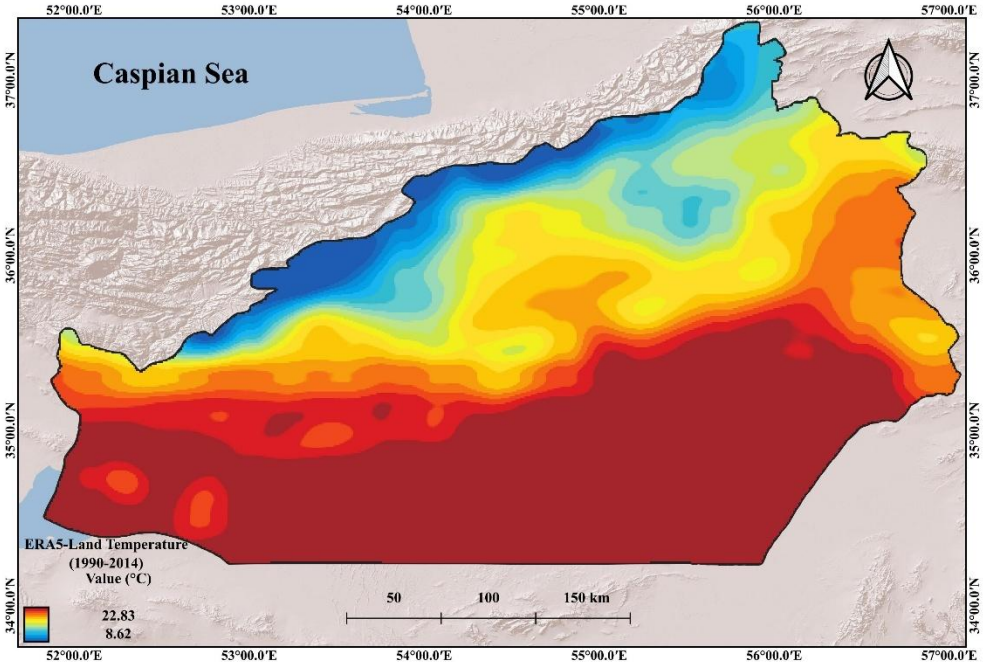


Figure_3 Map of mean annual temperature values based on bias corrected ERA5-Land reanalysis data in the study area during the baseline period (1990–2014)

3.2 Evaluation of Bias-Correction Accuracy in Climate Models

In this study, to assess the accuracy of bias correction for future data, historical data (1990–2014) were first used to bias-correct the climate model outputs. Since climate models project temperature data from 2015 to 2100 under various scenarios, their bias corrected outputs for the period 2015–2020 (where bias-corrected ERA5-Land reference data are available) were compared with the reference data. A high level of agreement between the two datasets during this evaluation period indicates that the bias-correction procedure is robust and can be reliably applied to future projections. Table 3 presents the statistical metrics between the temperature maps of the study area and the ensemble mean of the bias-corrected climate models under two scenarios for the period 2015–2020. The comparison was performed directly on the ensemble mean after bias correction. To statistically evaluate the relationship between the bias-corrected model ensemble and the ERA5-Land reference data during the study period, temperature values were first extracted from all maps, and then the relevant statistics were calculated. The results demonstrate strong agreement between the ERA5-Land reference data and the bias-corrected climate model ensemble outputs in both scenarios. The r value between the ERA5-Land reference data and the model ensemble outputs under SSP2-4.5 and SSP5-8.5 was 0.98 and 0.97, respectively. Additionally, the RMSE

between the reference temperature maps and the model ensemble means under SSP2-4.5 and SSP5-8.5 was 0.19 °C and 0.61 °C annually, respectively. These results indicate that the average model error in estimating annual temperature was consistently below 1 °C, which is considered acceptable for regional-scale temperature projections. Slightly better agreement was observed under the SSP2-4.5 scenario compared to SSP5-8.5 during the evaluation period.

Table 3. Statistical metrics calculated between the ensemble mean of climate model maps and the downscaled and bias-corrected ERA5-Land maps for the period 2015–2020 under SSP2-4.5 and SSP5-8.5 scenarios

Statistic	RMSE (°C)	Bias (°C)	r	MAE (°C)
SSP2-4.5	0.19	-0.02	0.98**	0.14
SSP5-8.5	0.61	0.25	0.97**	0.45

** indicates significant differences at $p < 0.01$.

3.3 Assessment of Projected Temperature Changes in the Study Area

The spatial distribution of mean annual temperature across the three future horizons, near (2025–2050), mid (2051–2075), and far (2076–2099), is illustrated in Figures 4 and 5 for the SSP2-4.5 and SSP5-8.5 scenarios, respectively. Under the intermediate SSP2-4.5 pathway, temperatures across the province are projected to range from 8.91–23.52 °C in the near-future, shifting to 9.63–24.44 °C in the mid-future, and ranging from 10.10 to 25.07 °C by the far-future. These results indicate a progressive thermal escalation, with warming becoming more pronounced in the far-future period. Mean provincial temperatures for these successive periods are estimated at 20.54 °C, 20.53 °C, and 22.11 °C, respectively. Notably, temperature increases are modest between the near- and mid-future periods but accelerate thereafter, representing an approximate overall rate of 1.0 °C every 30 years across the three future horizons within the study area.

Under the high-emission SSP5-8.5 scenario, Semnan Province is projected to experience a substantial and progressive thermal escalation across all future horizons. Annual temperature ranges are expected to shift from 9.11–23.76 °C in the near-future (2025–2050) to 10.27–25.48 °C in the mid-future (2051–2075), eventually reaching 11.86–27.53 °C by the far-future (2076–2099). Correspondingly, mean annual temperatures for these three periods are projected at 20.84 °C, 22.43 °C, and 24.31 °C, respectively. These results indicate a robust warming trend of approximately 2.0 °C every 30 years, representing a substantially stronger climatic signal compared to the SSP2-4.5 scenario.

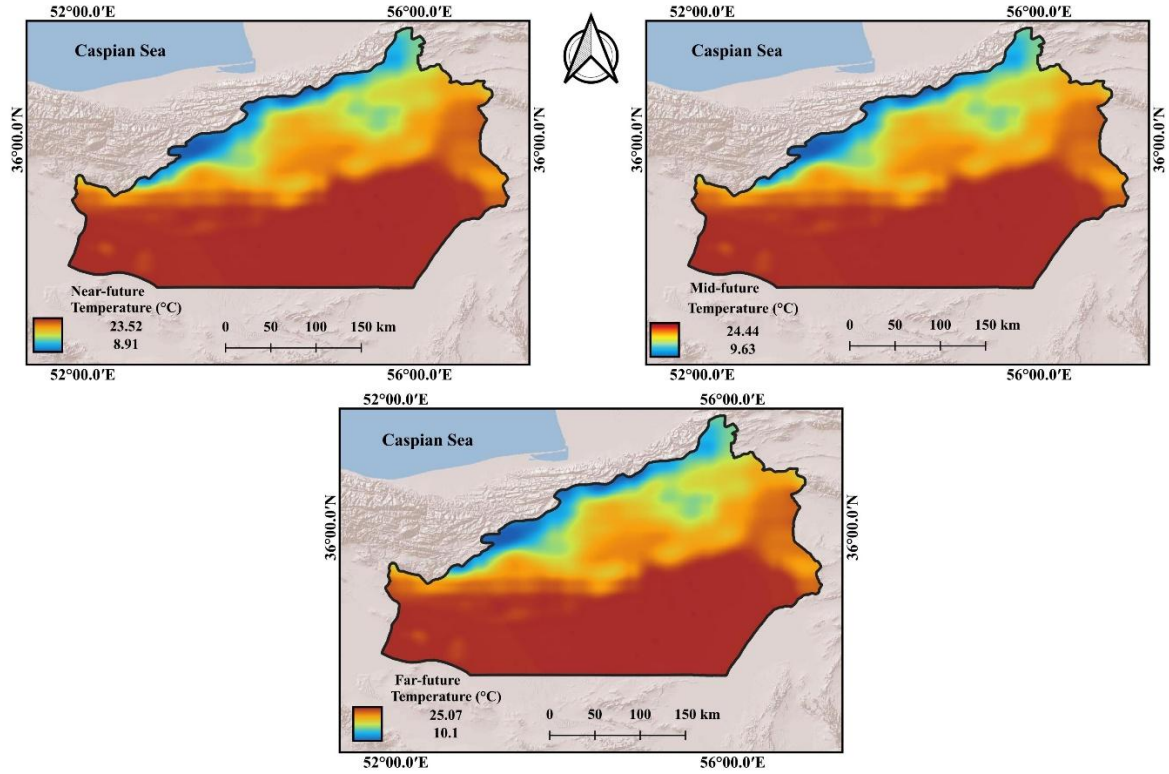


Figure_4 Spatial distribution of temperature in the study area in the near future (2025–2050), mid future (2051–2075), and far future (2076–2099) under the SSP2-4.5 scenario

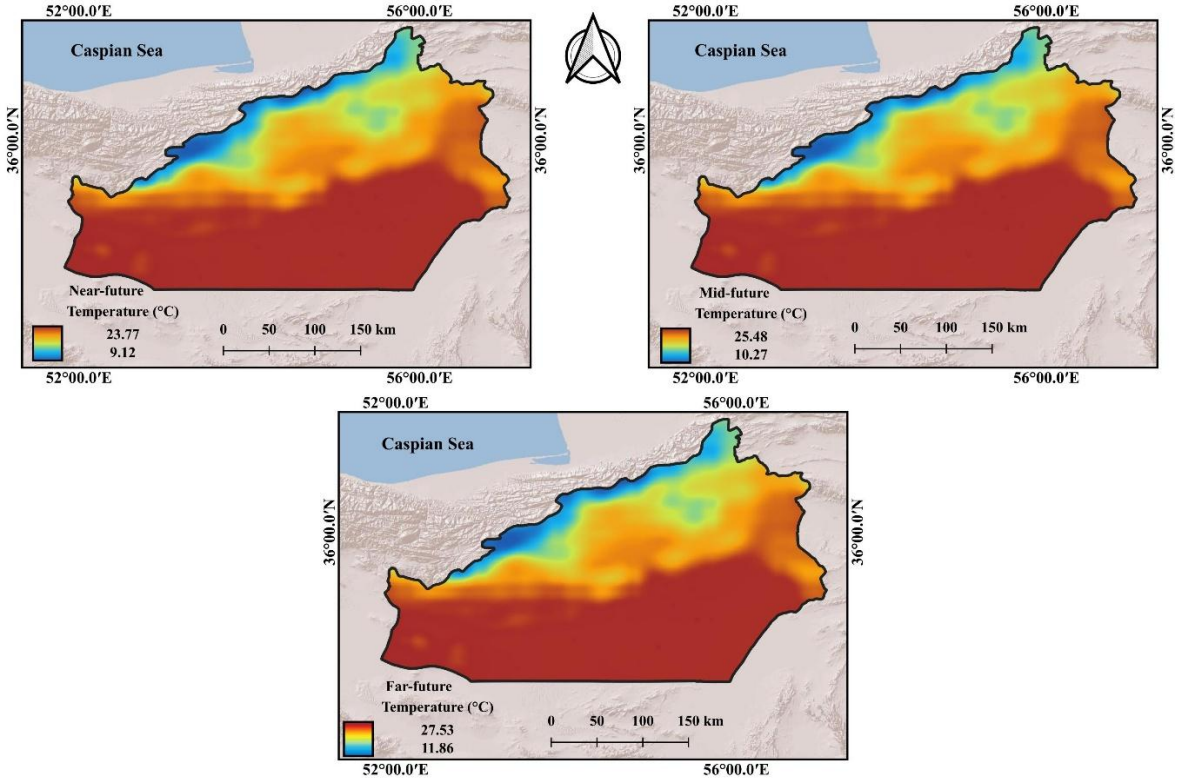


Figure_5 Spatial distribution of temperature in the study area in the near future (2025–2050), mid future (2051–2075), and far future (2076–2099) under the SSP5-8.5 scenario

To evaluate the impacts of climate change on temperature in the study area, the annual temperature distribution in the near, mid, and far future periods was analyzed using box plots. Figure 6 illustrates the distribution of temperature changes under the two SSP scenarios from CMIP6 models. In the baseline period, the median temperature was around 20 °C, with the first and third quartiles (Q_1–Q_3) ranging from approximately 18 to 22 °C. Under the intermediate scenario (SSP2-4.5), a moderate temperature increase is observed in the region. In this scenario, the median temperature reaches about 20.5–21 °C in the near future, 21–22 °C in the mid future, and 22–23 °C in the far future. The first and third quartiles gradually shift upward (from 19 to 24 °C in the far future), with only minor changes in the number and position of outliers, indicating steady warming with limited alteration to the existing spatial heterogeneity. This overall increase (about 2–3 °C relative to baseline) aligns with global emission reduction policies and exerts less pressure on water resources.

The high-emission scenario (SSP5-8.5) shows more severe temperature changes in the study area (Figure 6). In this scenario, the median temperature reaches 21.5 °C in the near future, 22.5–23 °C in the mid future, and 24–25 °C in the far future. The first and third quartiles become much wider (reaching 22 to over 25 °C in the far future), with a notable increase in high outliers, indicating greater spatial heterogeneity and contrast in temperature across the province. The overall temperature increase (more than 4–5 °C relative to baseline) is consistent with IPCC (2021) reports and could lead to intensified droughts, reduced soil moisture, and greater pressure on groundwater resources in Semnan Province.

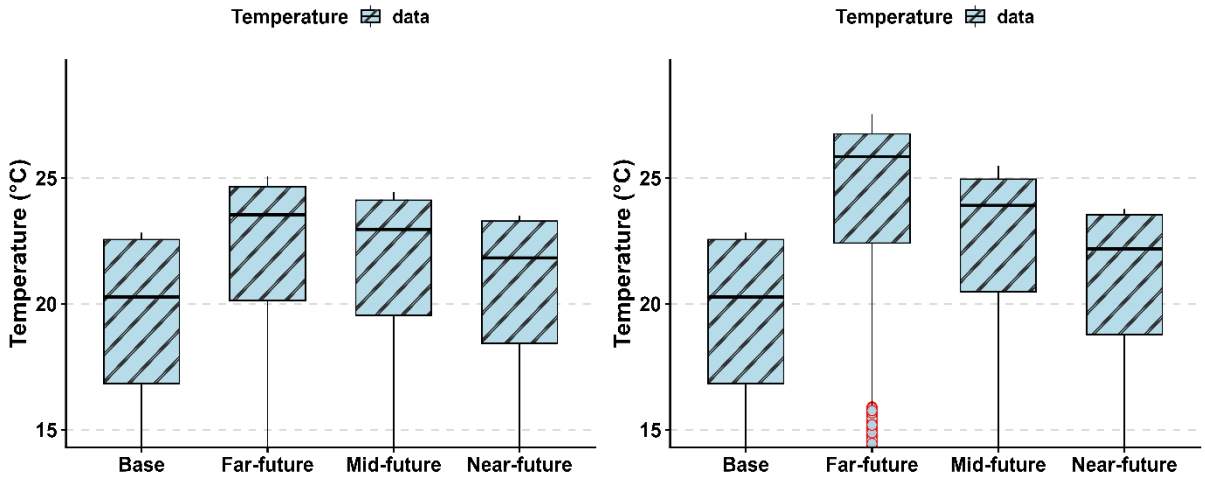


Figure_6 Box plot of projected temperature changes compared to the baseline period in the study area under SSP2-4.5 (left) and SSP5-8.5 (right) scenarios

Figure 4 shows the spatial distribution of temperature in the study area under the SSP2-4.5 scenario in the near, mid, and far future. In this scenario, the mean temperature changes (ΔT) relative to the baseline in the near, mid, and far future are projected to be 1.23 °C, 2.22 °C, and 2.80 °C, respectively. The spatial pattern shows a clear south-to-north gradient, with mountainous northern areas experiencing greater temperature increases. The maximum temperature changes in the near, mid, and far future are 1.88 °C, 3.04 °C, and 3.70 °C, respectively, while the minimum changes are 0.26 °C, 0.98 °C, and 1.48 °C. These results indicate that temperature changes will be more pronounced in the mid and far future under this scenario.

Figure 5 shows the spatial distribution of temperature in the study area under the SSP5-8.5 scenario in the near, mid, and far future. The mean temperature changes in this scenario for the near, mid, and far future are projected to be 1.53 °C, 3.13°C, and 5.00 °C, respectively, indicating a rapid and nonlinear increase in temperature. The median temperature changes in the studied futures under this scenario are 1.85 °C, 3.56 °C, and 5.48 °C, respectively. These results show that in the last 30 years of the current century, more than 50% of the areas in the province will experience temperature increases exceeding 5 °C. Additionally, the results indicate that northern areas of the study region, located at higher elevations along the southern slopes of the Alborz mountain ranges, will experience more intense warming. This pattern is consistent with elevation-dependent warming processes, likely driven by topographic land–atmosphere interactions.

3.4 Temperature Sensitivity of the Penman–Monteith Model

In this study, building on the methodology detailed in the Methods section, the sensitivity coefficients of the Penman-Monteith model to climatic variables (minimum, maximum, and mean temperature) were first evaluated on a daily basis and subsequently aggregated to the annual scale. Future ET_0 projections were then performed by scaling the baseline ET_0 values to the relative change in temperature, weighted by the corresponding sensitivity coefficient, applied at each grid cell. The annual sensitivity coefficients for maximum and minimum temperature variables in hyper-arid, arid, and semi-arid climates (consistent with the study area) are presented in Table 4. The results show that the sensitivity coefficients for both minimum and maximum temperature are positive, indicating a direct relationship between ET_0 and temperature. Moreover, the sensitivity coefficient for maximum temperature is larger than that for minimum temperature, suggesting a

greater influence of maximum temperature on ET_0. Given the focus of the present study on changes in mean temperature and their impact on ET_0, the average of all sensitivity coefficients (computed daily and aggregated annually across the study area) was calculated, yielding a mean sensitivity coefficient of 0.6 for annual mean temperature (Table 4). This implies that a 10% increase in air temperature leads to an approximate 6% increase in ET_0.

Equivalently, considering a regional mean annual temperature of approximately 20.5 °C, this corresponds to an approximate 3% increase in ET_0 per 1 °C of warming, assuming near-linear behavior within the analyzed range. Although the study area exhibits strong north–south gradients and spans hyper-arid to semi-arid climate regimes, the sensitivity coefficients showed only moderate variability across these zones (Table 4). Therefore, a single regionally averaged coefficient of 0.6 was adopted to ensure methodological consistency and avoid introducing additional uncertainty associated with spatially heterogeneous sensitivity estimates. Spatial variability in projected ET_0 is instead captured through the high-resolution gridded temperature changes, which represent the dominant driver of ET_0 variability in the study region.

Table 4. Annual sensitivity coefficients of climatic variables to ET_0 in different climates

Climate	Mean	T_{max}	T_{min}
Hyper-arid	0.76	1.23	0.29
Arid	0.56	0.92	0.19
Semi-arid	0.46	0.78	0.14

3.5 Baseline ET_0 Estimation

Given the sensitivity of ET_0 to temperature variations, future ET_0 projections were performed by applying the derived sensitivity coefficients to projected temperature changes at each grid cell. To enable this step, the spatial distribution of mean annual ET_0 during the baseline period (1990-2014) was first determined. In this study, ET_0 was estimated using the RF model with key meteorological predictors, including maximum and minimum air temperature, solar radiation, wind speed, and relative humidity. These predictors were derived from bias-corrected ERA5-Land, calibrated against ground-based synoptic observations, ensuring consistency between gridded inputs and station-based measurements.

Figure 7 shows the scatter plot of measured versus predicted ET_0 values. The data points lie close to the 1:1 line ($y = x$), indicating a strong correlation between the model predictions and measured values ($r = 0.98$, $R^2 = 0.96$, $p < 0.001$). Additionally, the model's RMSE for annual ET_0 estimation

was 104 mm/year, corresponding to approximately 7% of the mean annual ET_0, which demonstrates high predictive accuracy and robustness of the RF model in reproducing spatial ET_0 variability.

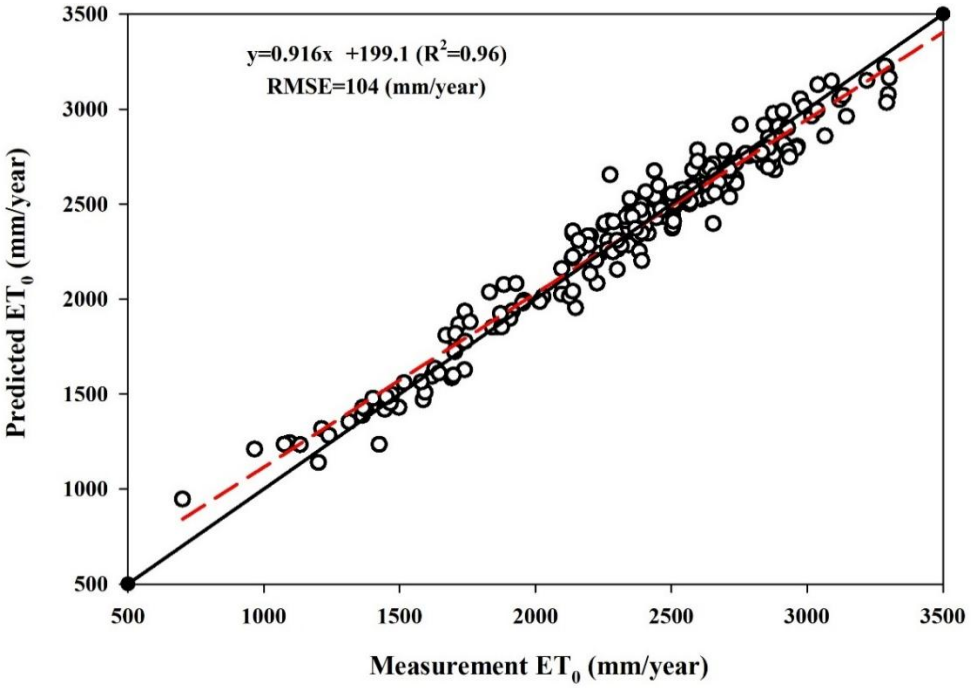


Figure_7 Annual measured and predicted ET_0 values in the baseline period

Figure 8 illustrates the spatial distribution of mean annual ET_0 in the study area during the baseline period. ET_0 ranges approximately from 1000 to 3200 mm $year^{-1}$, reflecting substantial climatic heterogeneity across the region. Based on the RF model outputs, lower evapotranspiration rates are observed in the northern parts of the province, whereas maximum ET_0 values occur in the eastern and southern areas, which correspond to low-elevation and desert regions.

This spatial pattern is consistent with the north–south temperature gradient and elevation controls shown in Figure 3. Higher temperatures and lower elevations enhance atmospheric evaporative demand, leading to increased ET_0 in southern and eastern sectors, while cooler conditions and higher elevations in the north constrain evapotranspiration rates.

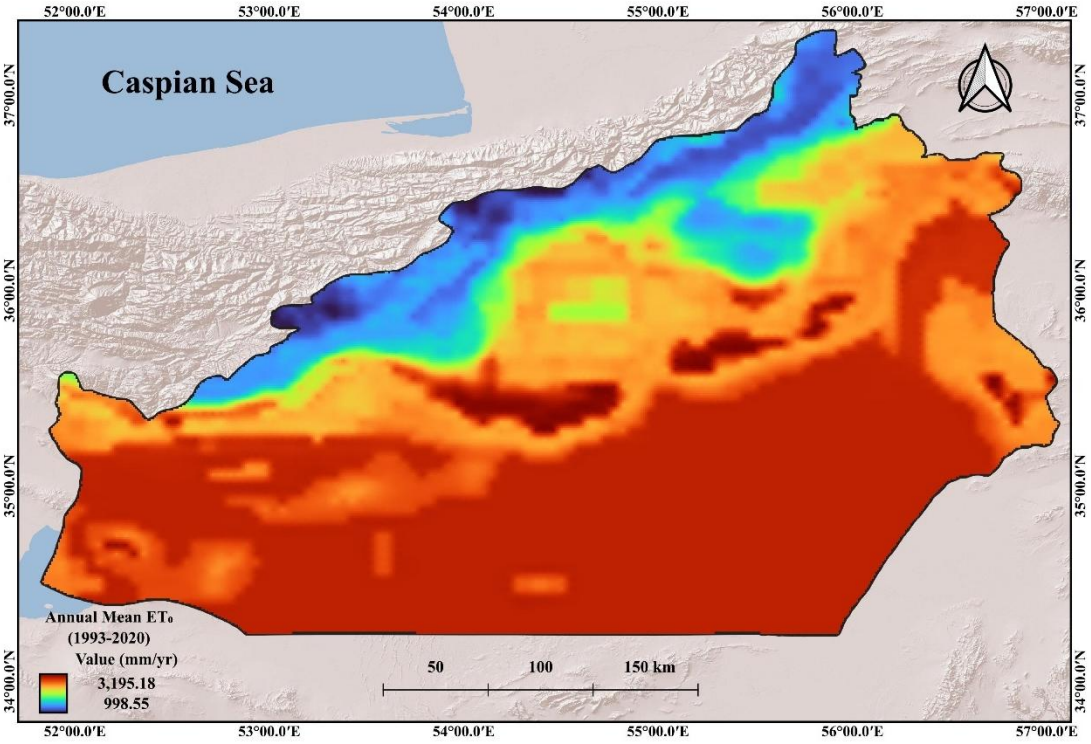


Figure_8 Mean annual reference evapotranspiration (ET_0) in the study area (1990–2014). The spatial pattern broadly follows the north–south temperature gradient and elevation controls shown in Figure 3.

3.6 Future Projections of ET_0

Based on the results shown in Figure 9, the minimum annual ET_0 values in Semnan Province during the baseline period were approximately 1000 mm year^{-1}, while minimum ET_0 values in future periods under both scenarios show consistent increases. Under the SSP2-4.5 scenario, the minimum ET_0 values are projected to reach 1020 mm year^{-1}, 1070 mm year^{-1}, and 1095 mm year^{-1} in the near, mid-, and far-future periods, respectively. These results indicate an overall increase of approximately 95 mm in minimum ET_0 from the baseline to the far future over the next 75 years. The mean ET_0 under this scenario is projected to increase to 2686 mm year^{-1}, 2764 mm year^{-1}, and 2804 mm year^{-1} in the near, mid-, and far-future periods, respectively, compared to the baseline mean of 2590 mm year^{-1}. This corresponds to an average increase of approximately 215 mm over 75 years (≈2.85 mm year^{-1}).

The first quartile of ET_0, representing cooler and higher-elevation areas, increases from 2485 mm year^{-1} during the baseline period, to 2600 mm year^{-1}, 2695 mm year^{-1}, and 2740 mm year^{-1}, respectively, across the three future horizons. This indicates that relatively cooler regions exhibit stronger relative increases in ET_0, reflecting their higher sensitivity to projected warming. Thus,

the SSP2-4.5 scenario suggests a moderate but spatially heterogeneous increase in ET0, driven primarily by gradual temperature rise.

According to Figure 10, the intensity of ET_0 changes under the SSP5-8.5 scenario is more severe. In this scenario, the mean ET_0 in the study area is projected to reach 2706 mm year^{-1},, 2831 mm year^{-1}, , and 2978 mm year^{-1}, in the near-, mid-, and far-future, respectively.

This represents an overall increase of approximately 388 mm from the baseline to the far future over 75 years, equivalent to an average rise of about 5.2 mm year^{-1}. The first quartile increases to 2627 mm year^{-1}, 2768 mm year^{-1}, and 2927 mm year^{-1} in the near-, mid-, and far-future periods, respectively. These results indicate a pronounced upward shift of the entire ET_0 distribution under the SSP5-8.5 scenario, reflecting intensified atmospheric evaporative demand across all climatic zones. Such increases may enhance the risk of moisture deficits and drought stress, particularly in regions already characterized by arid or semi-arid climatic conditions.

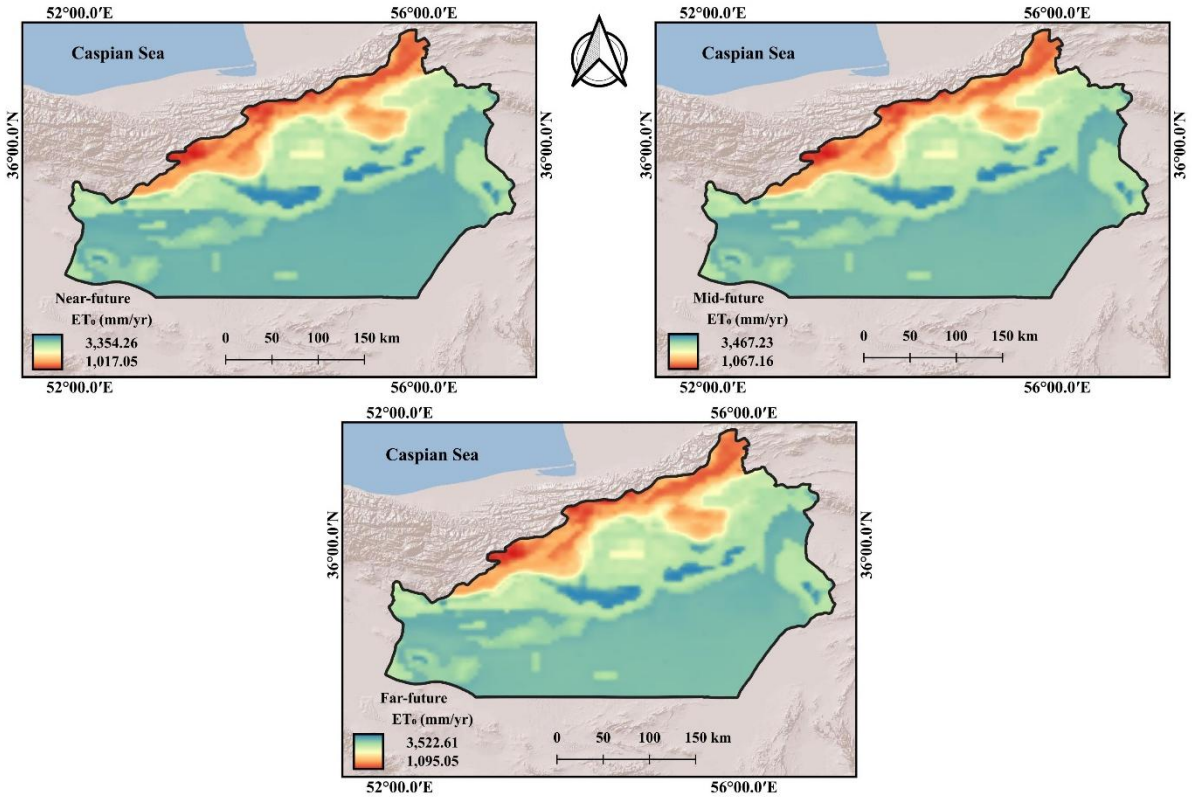


Figure_9 Mean annual reference evapotranspiration (ET_0) values in Semnan Province during the near future (2025–2050), mid future (2051–2074), and far future (2075–2099) periods under the SSP2-4.5 scenario

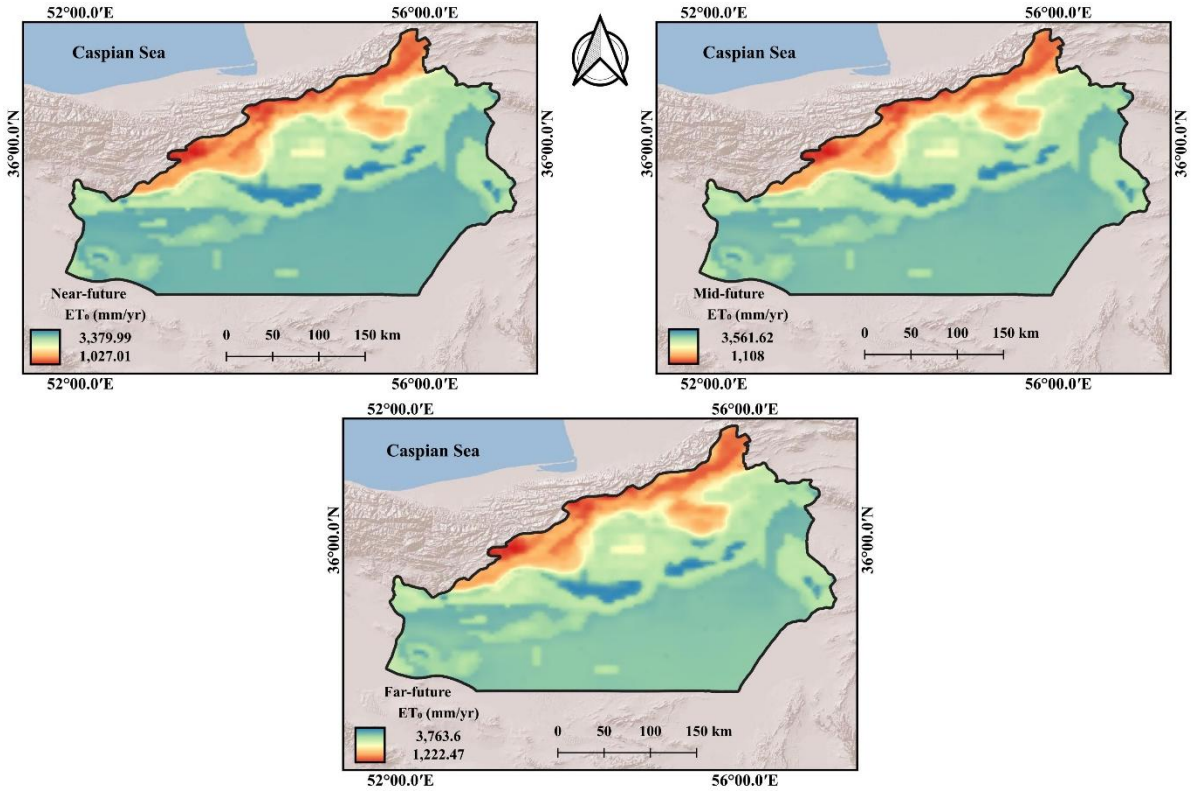


Figure_10 Mean annual reference evapotranspiration (ET_0) values in Semnan Province during the near future (2025–2050), mid future (2051–2074), and far future (2075–2099) periods under the SSP5-8.5 scenario

Figures 11 and 12 illustrate the spatial distribution of changes in mean annual reference evapotranspiration (ΔET_0) relative to the baseline period, defined as the difference in mean annual ET_0 (mm year^{-1}) between each future period and the baseline period, in Semnan Province for the three future time periods (near: 2025–2050, mid: 2051–2074, far: 2075–2099) under the SSP2-4.5 and SSP5-8.5 scenarios.

According to the results, ΔET_0 is positive across all regions of the province in both scenarios, indicating an increase in ET_0 compared to the baseline. Under the SSP2-4.5 scenario, the near future shows an average increase ranging from 9 to 160 mm. Changes in ET_0 in the mid future range from 61 to 287 mm, and in the far future from 85 to 345 mm. The results also indicate that the northern and central parts of the province will experience the greatest increases in ET_0. The median values of ΔET_0 under this scenario in the near, mid, and far future are 101 mm, 180 mm, and 219 mm, respectively, indicating that more than 50% of the province experiences an increase exceeding 219 mm by the far-future period.

Under the SSP5-8.5 scenario (Figure 12), changes in ET_0 exhibit more intense patterns. In the near future, ΔET_0 ranges from 20 to 198 mm, in the mid future from 98 to 385 mm, and in the far future

from 207 to 598 mm. The average increase in ET_0 under this scenario in the near-, mid-, and far-future is 109 mm, 234 mm, and 385 mm, respectively. This corresponds to an average increase of approximately 16% in the far future relative to the baseline.

Spatially, the largest increases in ET_0 occur in the northern and central parts of the province, which are characterized by higher elevation and greater agricultural activity. This pattern suggests that areas currently supporting the majority of agricultural production are likely to experience the most significant increases in atmospheric evaporative demand.

Conversely, desert and sparsely vegetated regions show relatively smaller absolute changes, reflecting lower baseline ET_0 sensitivity despite higher temperatures.

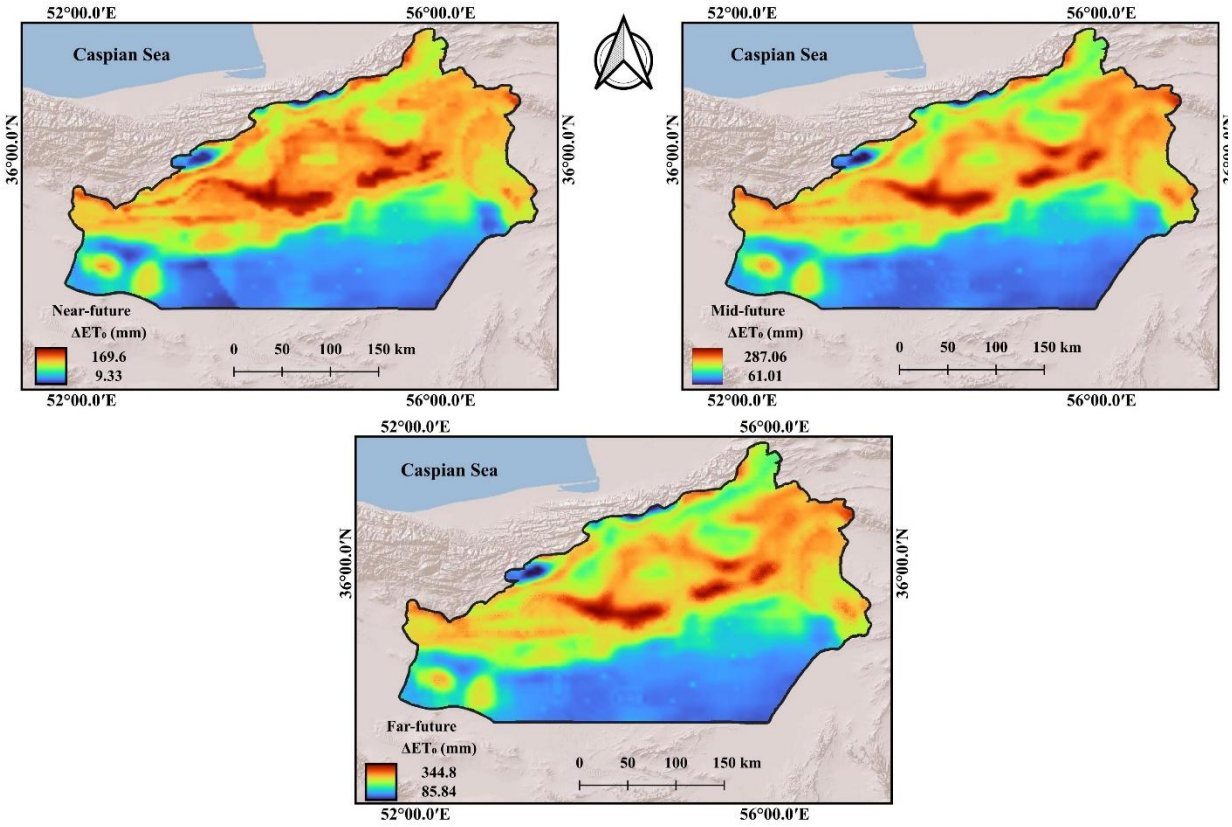


Figure_11 Spatial distribution of differences in ET_0 relative to the baseline period (ΔET_0) in the study area during the near future (2025–2050), mid future (2051–2074), and far future (2075–2099) periods under the SSP2-4.5 scenario

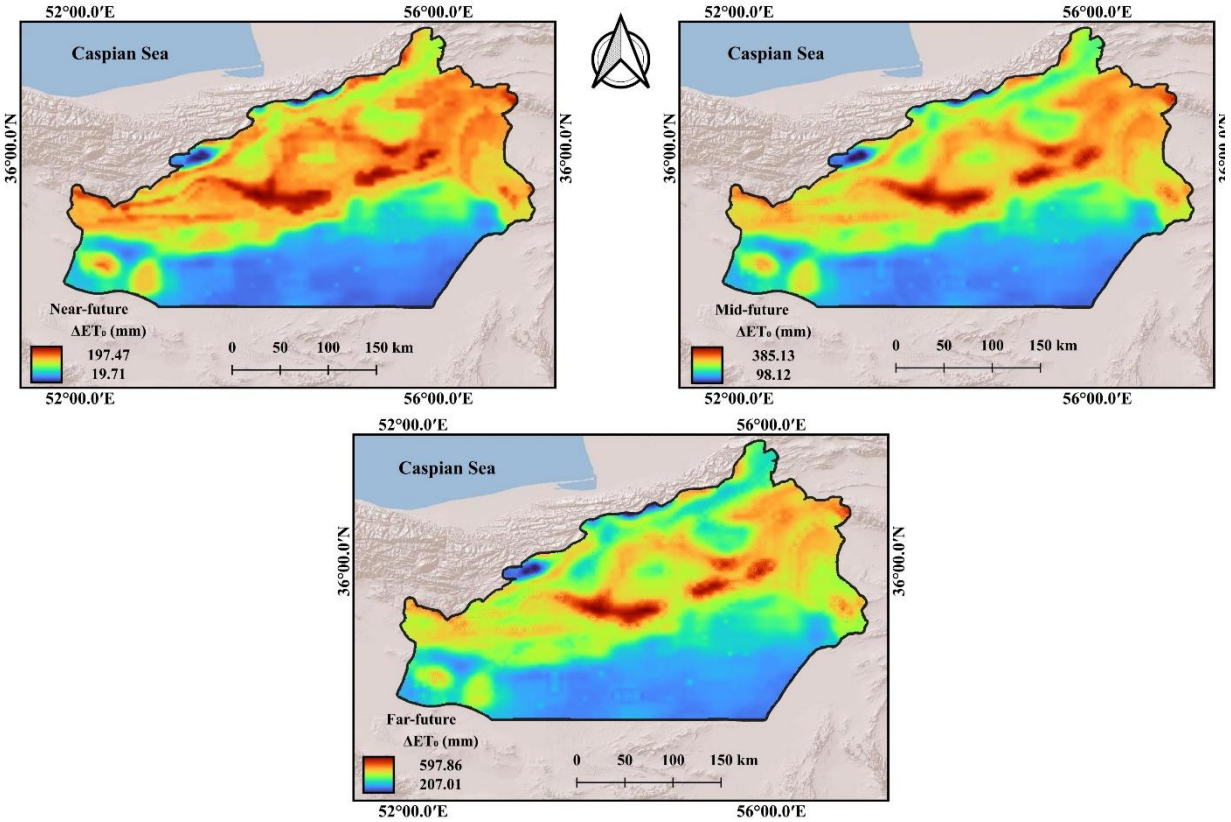


Figure_12 Spatial distribution of differences in ET_0 relative to the baseline period (ΔET_0) in the study area during the near future (2025–2050), mid future (2051–2074), and far future (2075–2099) periods under the SSP5-8.5 scenario

4. Discussion

4.1 Main Findings Compared to Literature

In the present study, an approximate annual increase of 2.8 mm/year in ET_0 was projected under the SSP2-4.5 scenario and 5.2 mm/year under SSP5-8.5 (with overall rises of 6.5% and 10%, respectively, over 2025–2099), consistent with several previous studies on temperature-driven changes in reference evapotranspiration. Similarly, Sobh (2025), using CMIP6 models under SSP scenarios in arid Egypt, projected ET_0 increases ranging from 4.36% (SSP1-2.6 near future) to 14.2% (SSP5-8.5 far future), attributing ~80% to warming, which aligns with the thermal sensitivity coefficient of 0.6 obtained in this study, which suggests an approximate 6% ET_0 increase for every 10% rise in annual air temperature. This methodological approach is consistent with Nasrollahi et al. (2021), who utilized the dimensionless sensitivity coefficient method across 50 synoptic stations in Iran to evaluate the influence of climatic variables on ET_0 in diverse climates. Likewise, Deveci and Konukcu (2024) in Turkey's Thrace region, using the RegCM3 model under the A2 scenario, projected ET_0 increasing from 3.3 mm/day in the reference period

(1970–1990) to 3.4, 3.6, and 4.0 mm/day in the short-, mid-, and long-term periods (up to 2085), indicating a sensitivity of 0.1 mm/day (4%) per 1 °C of warming. The results of Modaresi and Araghi (2023), who projected daily station data, showed that under the SSP5-8.5 scenario, ET_0 is expected to increase by an average of approximately 0.9 mm/day across all stations during 2061–2090 (especially on hot days), with higher rates in arid and semi-arid environments. These findings are also consistent with Nouri and Veysi (2024), who reported an increasing trend in ET_0 across Iran and projected that, during 2030–2049, ET_0 would increase by an average of 4.8% under SSP2-4.5 and 5.3% under SSP5-8.5 relative to the baseline (1985–2014). They further projected larger increases during 2080–2099, with mean ET_0 increases of 8.0% and 13.3% under SSP2-4.5 and SSP5-8.5, respectively. The findings of the present study are also in agreement with Ajjur and Al-Ghamdi (2021), who projected ET_0 increases of 0.37 mm/year in the mid-century (2021–2050) and 0.51 mm/year by the end of the century (2071–2100) under SSP2-4.5 and SSP5-8.5. In South America, Gondim et al. (2018), based on CMIP5 climate models, reported ET_0 increases of 2.3%–6.3% by 2025–2055 and indicated that irrigation water demand would rise by 2.8%–16.7% under these conditions. It has also been widely reported that global patterns of ET_0 change exhibit spatial heterogeneity: the rate of increase in ET_0 is higher in semi-arid areas than in fully arid zones, resulting in greater ecosystem vulnerability.

4.2 Methodological Contribution

Our use of bias-corrected ERA5-Land reanalysis data, downscaled with RF, enhances both spatial resolution and accuracy of ET_0 projections in data-sparse regions like Semnan Province (as detailed in the Results). Due to the coarse resolution of global climate model (GCM) data, direct application requires downscaling and bias correction; researchers often evaluate outputs at stations and use interpolation (e.g., kriging) for sparse areas. In this study, ERA5-Land reanalysis data (9 km resolution) were downscaled via kriging and bias-corrected using RF against synoptic stations, serving as a validated high-resolution gridded reference for regional-scale investigations. The results showed substantial bias in raw ERA5-Land temperatures (RMSE 2.35 °C, bias +1.70 °C), reduced post-correction (RMSE 1.00 °C, bias −0.01 °C), enabling its use as a gridded proxy for observations. This approach improves spatial accuracy of future projections by aligning GCM ensembles with bias-corrected ERA5-Land, outperforming station-only methods in data-sparse arid regions. This aligns with Raeesi et al. (2024), who applied quantile mapping and RF for bias

correction of ERA5-Land precipitation and CMIP6 outputs over Iran, improving accuracy by ~20%, while Zolfaghari et al. (2025) combined corrected reanalysis with machine learning for enhanced ET_0 estimation. Gourgouletis, Gkavrou, and Baltas (2023) confirmed bias correction boosts ERA5-Land's ET_0 accuracy. Our integration of RF for bias correction and sensitivity-based ET_0 scaling demonstrates that corrected reanalysis can effectively bridge GCM limitations, providing reliable gridded projections.

4.3 Implications for Water Management

Raeesi et al. (2024) reported projected precipitation reductions (>10%) in many arid and semi-arid regions of Iran under SSP scenarios (e.g., central and eastern declines under SSP5-8.5); therefore, rising temperatures and ET_0 are expected to make the climate of these areas drier, thereby increasing crop water requirements. Our findings indicate higher atmospheric evaporative demand from ET_0 increases, potentially elevating crop evapotranspiration ($ET_c = ET_0 \times Kc$) and irrigation needs if crop coefficient (K_c) and management remain constant, although actual ET_c depends on specific K_c, soil management, and water availability. This change is particularly relevant in semi-arid regions such as Semnan Province, where it can place considerable pressure on water resources. Increased ET_0 also means greater evaporation losses from reservoirs, dams, and surface water bodies, posing a serious threat to food and water security under conditions of water scarcity. Overall, the findings of this research highlight the need for adaptive water resource management, including efficient irrigation practices, adjustments in cropping patterns, and localized modeling using corrected data.

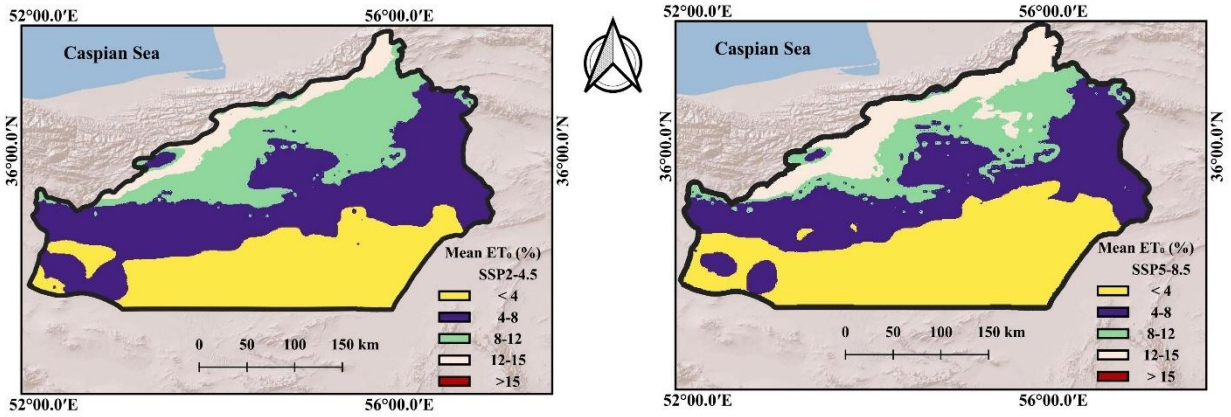


Figure 13. Mean percentage change in ET_0 relative to the baseline period under the SSP2-4.5 and SSP5-8.5 scenarios during 2025–2099 in the study area

4.4 Limitations of the Study

Although this study produced promising results, several limitations should be noted. ET_0 depends on several climate variables, including T, RH, and wind speed. These variables are also expected to change under future climate conditions. In this study, we assumed that only air temperature would vary, and we projected ET_0 based on this assumption. However, other variables, such as wind speed, carry high uncertainty in future projections. Including these variables would therefore increase the overall uncertainty in the projected ET_0. The use of ERA5-Land data, while useful for large-scale estimates, also has drawbacks related to the accuracy of certain meteorological variables. For instance, (Vanella et al. 2022), (Ippolito et al. 2024), and (Zolfaghari et al. 2025), found that ERA5-Land estimates of relative humidity and wind speed often differ significantly from ground-based station measurements. The native spatial resolution of ERA5-Land data is approximately 9 km, which can be downscaled to 1 km. This finer resolution works well for flat terrain but may introduce greater uncertainty in areas with complex topography, such as the northern part of the study region. Achieving higher accuracy for ET_0 in such areas would require even finer resolution data. Finally, the study also focused on annual ET_0 trends and sensitivity coefficients, drawing from historical station data (1990–2014) and projections up to 2099. This approach provides valuable insights into long-term patterns but overlooks seasonal or daily variations, which are particularly pronounced in arid regions during hot periods.

5. Conclusion

This research provides a robust spatiotemporal projection of ET_0 in Semnan Province, Iran, by integrating an ensemble of five CMIP6 climate models with RF machine learning and the FAO Penman-Monteith methodology. The five models were selected based on their performance in simulating temperature and precipitation in arid and semi-arid regions, but a limitation is that results may be sensitive to model choice due to inter-model variability in CMIP6; future studies could expand the ensemble to test this sensitivity. The study successfully addressed regional data limitations by utilizing bias-corrected ERA5-Land reanalysis data as a locally validated high-resolution (1 km) reference after bias-correction, which served as an effective proxy for ground-based observations after validation against regional synoptic stations. The results consistently indicate a warming trend across all future time horizons, near (2025–2050), mid (2051–2075), and far (2076–2099), with mean annual temperatures projected to rise by approximately 1.0 °C every 30 years under the intermediate SSP2-4.5 scenario and a more aggressive 2.0°C every 30 years under the high-emission SSP5-8.5 scenario. These thermal increases serve as the primary catalyst

for rising evaporative demand, as sensitivity analysis identified mean temperature as the dominant driver with an annual sensitivity coefficient of 0.6.

The methodological framework demonstrated that bias-corrected reanalysis data enhance spatial accuracy in data-sparse arid regions, as evidenced by the high correlation (r = 0.98) between the ensemble mean and the reference data during the validation period. By utilizing a multi-model ensemble, the study reduces dependence on a single model and partially addresses model uncertainty, providing a more reliable range of outcomes than single-model approaches. Consequently, ET_0 is projected to increase by 2.85 mm/year under the intermediate pathway and 5.2 mm/year under the high-emission scenario, culminating in a total rise of up to 16% relative to the baseline by the end of the century.

Spatially, the most intense ET_0 increases are concentrated in the northern and central regions, which encompass the province's primary agricultural lands, rather than the southern desert zones. This spatial heterogeneity suggests that the area is most critical for regional food security face the highest risk of future moisture deficits and intensified drought stress. Ultimately, these findings reveal that accelerating evaporative demand will lead to a critical moisture imbalance. This scientific assessment underscores an urgent necessity for adaptive water resource management, highlighting that optimized irrigation strategies, improved water-saving technologies, and localized adjustments in regional cropping patterns are essential to maintain agricultural productivity and ecological resilience throughout the 21st century.

Author Contributions Ali Asghar Zolfaghari: Conceptualization, Data curation, Formal Analysis, Methodology, Software, Validation, Visualization, Maryam Raeesi: Conceptualization, Visualization, Writing, Reviewing, and Editing. Giuseppe Longo-Minnolo: Conceptualization, Writing, Reviewing, and Editing. Azade Soltani: Conceptualization, Writing, and Editing. Davoud Kartoulinezhad: Conceptualization, Writing, and Editing.

Data Availability Data and materials developed by the authors are available upon request.

Declarations

Consent to Publish All authors approve the publication in this journal.

Conflict of Interest The authors declare no conflict of interest.

Ethical Approval Not applicable

Financial Interests The authors declare they have no financial interests.

Funding No funding was received to assist with the preparation of this manuscript.

References

Ahmadalipour, Ali, Arun Rana, Hamid Moradkhani, and Ashish Sharma. 2017. "Multi-Criteria Evaluation of CMIP5 GCMs for Climate Change Impact Analysis." *Theoretical and Applied Climatology* 128(1–2):71–87. doi:10.1007/s00704-015-1695-4.

Ajjur, Salah Basem, and Sami G. Al-Ghamdi. 2021. "Evapotranspiration and Water Availability Response to Climate Change in the Middle East and North Africa." *Climatic Change* 166(3–4):28. doi:10.1007/s10584-021-03122-z.

Alaminie, Addis A., Seifu A. Tilahun, Solomon A. Legesse, Fasikaw A. Zimale, Gashaw Bimrew Tarkegn, and Mark R. Jury. 2021. "Evaluation of Past and Future Climate Trends under CMIP6 Scenarios for the UBNB (Abay), Ethiopia." *Water* 13(15):2110. doi:10.3390/w13152110.

Allen, Richard G., Luis S. Pereira, Dirk Raes, and Martin Smith. 1998. "Crop Evapotranspiration-Guidelines for Computing Crop Water Requirements-FAO Irrigation and Drainage Paper 56." *Fao, Rome* 300(9):D05109.

Beven, Keith. 1979. *A Sensitivity Analysis of the Penman-Monteith Actual Evapotranspiration Estimates*. Vol. 44. Elsevier.

Cheshmberah, Fatemeh, and Ali Asghar Zolfaghari. 2019. "The Effect of Climate Change on Future Reference Evapotranspiration in Different Climatic Zones of Iran." *Pure and Applied Geophysics* 176(8):3649–64. doi:10.1007/s00024-019-02148-w.

Cook, Benjamin I., Toby R. Ault, and Jason E. Smerdon. 2015. "Unprecedented 21st Century Drought Risk in the American Southwest and Central Plains." *Science Advances* 1(1):e1400082. doi:10.1126/sciadv.1400082.

Deveci, Huzur, and Fatih Konukcu. 2024. *Modeling the Effect of Climate Change on Evapotranspiration in the Thrace Region*. Vol. 15. MDPI AG.

Disasa, Kinde Negessa, Haofang Yan, Rongxuan Bao, Jianyun Zhang, Chuan Zhang, Biyu Wang, and Guoqing Wang. 2025. *Modelling the Impacts of Future Climate Variable Changes on Rainfed Maize Production, Evapotranspiration, and Adaptation Measures in Northeast China*. Elsevier.

Frederick, Kenneth D., and David C. Major. 1997. "Climate Change and Water Resources." *Climatic Change* 37(1):7–23. doi:10.1023/A:1005336924908.

Gondim, Rubens, Cleiton Silveira, Francisco De Souza Filho, Francisco Vasconcelos, and Daniel Cid. 2018. "Climate Change Impacts on Water Demand and Availability Using CMIP5 Models in the Jaguaribe Basin, Semi-Arid Brazil." *Environmental Earth Sciences* 77(15):550. doi:10.1007/s12665-018-7723-9.

Gou, Qiqi, Yonghua Zhu, Robert Horton, Haishen Lü, Zhenlong Wang, Jianbin Su, Chenyun Cui, Haoqiang Zhang, Xiaoyi Wang, and Jingyao Zheng. 2020. *Effect of Climate Change on the Contribution of Groundwater to the Root Zone of Winter Wheat in the Huaibei Plain of China*. Vol. 240. Elsevier.

Gourgouletis, Nikolaos, Marianna Gkavrou, and Evangelos Baltas. 2023. *Comparison of Empirical ET_0 Relationships with ERA5-Land and in Situ Data in Greece*. Vol. 3. MDPI.

Heravi, Hesam, and Ali-Asghar Zolfaghari. 2024. "Using Machine Learning Method to Estimate Evapotranspiration (Case Study: Semnan Province)." *Iranian Journal of Soil and Water Research* 55(5):781–97.

Heshmati, Ferdos, and Nasrin Sayari. 2021. "Projected Changes of Potential Evapotranspiration under RCP Climate Change Scenarios (Case Study: Bandar Anzali)." *Journal of Agricultural Meteorology* 9(1):63–76.

Hou, Haiyan, Xia Li, Yuanzhi Yao, Guohua Hu, Cheng Wang, and Nan Chu. 2025. *Attributing Future Changes in Terrestrial Evapotranspiration: The Combined Impacts of Climate Change, Rising CO2, and Land Use Change*. Vol. 373. Elsevier.

Huang, Na, Yu Song, Jialin Wang, Ziyuan Zhang, Shangqian Ma, Kang Jiang, and Zhihua Pan. 2022. *Climatic Threshold of Crop Production and Climate Change Adaptation: A Case of Winter Wheat Production in China*. Vol. 10. Frontiers Media SA.

IPCC. 2021. "Latest IPCC 6th Assessment Report | Polar Bears International." https://polarbearsinternational.org/news-media/articles/latest-global-climate-report?gad_source=1&gad_campaignid=23349892281&gbraid=0AAAADw5J6YECaCXZdslZE_KRktZhrbns&gclid=CjwKCAiA3-3KBhBiEiwA2x7FdDdEaopAnHlCE6MkKGectW3nMyOiMEpG8_Mo6DKpf417Q_1fBVNcKhoCc-QQAvD_BwE.

Ippolito, Matteo, Dario De Caro, Marcella Cannarozzo, Giuseppe Provenzano, and Giuseppe Ciraolo. 2024. *Evaluation of Daily Crop Reference Evapotranspiration and Sensitivity Analysis of FAO Penman-Monteith Equation Using ERA5-Land Reanalysis Database in Sicily, Italy*. Vol. 295. Elsevier.

Jain, Sharad K., and Vijay P. Singh. 2024. "Climate Change and Its Impacts on Water Resources." Pp. 793–829 in *Water Resources Systems Planning and Management*. Elsevier.

Jerin, Jannatun Nahar, H. M. Touhidul Islam, Abu Reza Md Towfiqul Islam, Shamsuddin Shahid, Zhenghua Hu, Mehnaz Abbasi Badhan, Ronghao Chu, and Ahmed Elbeltagi. 2021. "Spatiotemporal Trends in Reference Evapotranspiration and Its Driving Factors in Bangladesh." *Theoretical & Applied Climatology* 144(1/2):793. doi:10.1007/s00704-021-03566-4.

Karimi, Nasrolahi, and Iranshahi. 2024. "Investigating the Effects of Climate Change on Reference Evapotranspiration Based on the SSP Scenarios." *Iranian Journal of Soil and Water Research* 54(11):1759–77.

Lai, Chengguang, Xiaohong Chen, Ruida Zhong, and Zhaoli Wang. 2022. *Implication of Climate Variable Selections on the Uncertainty of Reference Crop Evapotranspiration Projections Propagated from Climate Variables Projections under Climate Change*. Vol. 259. Elsevier.

Liu, Q., F. Zhang, J. Chen, and Y. Li. 2020. "Water Stress Altered Photosynthesis-Vegetation Index Relationships for Winter Wheat." *Agronomy Journal* 112(4):2944–55. doi:10.1002/agj2.20256.

Liu, Wen, Yiyi Li, Dongfeng Li, Peirong Lin, Xiaoming Wang, Hamish D. Pritchard, and Philip DA Kraaijenbrink. 2025. *Impacts of Changes in Climate, Cryosphere, and Vegetation on Freshwater Supply in the Southeastern Tibetan Plateau*. Vol. 661. Elsevier.

Mirhosseiny, Seyed Mohammad Reza, Hoda Ghasemieh, and Khodayar Abdollahi. 2021. "Prediction of Monthly Potential Evapotranspiration under RCP Scenarios in Future Periods (Case Study: Golpayegan Basin)." *Journal of Ecohydrology* 8(1):205–20.

Modaresi, Fereshteh, and Alireza Araghi. 2023. *Projecting Future Reference Evapotranspiration in Iran Based on CMIP6 Multi-Model Ensemble*. Vol. 153. Springer Nature BV.

Najafi, H., Lagerwall, G. L., Obeysekera, J., & Liu, J. (2026). Machine learning in climate downscaling: A critical review of methodologies, physical consistency, and operational applications. *Water, 18*(2), Article 271. https://doi.org/10.3390/w18020271

Nasrollahi, Muhammad, Ali Asghar Zolfaghari, and Mohammad Reza Yazdani. 2021. "Spatial and Temporal Properties of Reference Evapotranspiration and Its Related Climatic Parameters in the Main Agricultural Regions of Iran." *Pure and Applied Geophysics* 178(10):4159–79. doi:10.1007/s00024-021-02806-y.

Nouri, Milad, and Shadman Veysi. 2024. *CMIP6 Multi-Model Ensemble Projection of Reference Evapotranspiration Using Machine Learning Algorithms*. Vol. 306. Elsevier.

Raeesi, Maryam, Ali Asghar Zolfaghari, Seyed Hasan Kaboli, Mohammad Rahimi, Joris de Vente, and Joris PC Eekhout. 2024. *Using Quantile Mapping and Random Forest for Bias-Correction of High-Resolution Reanalysis Precipitation Data and CMIP6 Climate Projections over Iran*. Vol. 44. John Wiley & Sons, Ltd. Chichester, UK.

Raeesi, Maryam, Ali Asghar Zolfaghari, Mohammad Reza Yazdani, Manouchehr Gorji, and Marmar Sabetizade. 2019. *Prediction of Soil Organic Matter Using an Inexpensive Colour Sensor in Arid and Semiarid Areas of Iran*. Vol. 57. CSIRO Publishing.

Sobh, M. T., Nashwan, M. S., Amer, N., & Shahid, S. (2024). Simulation and future projections of reference evapotranspiration in Egypt. International Journal of Climatology, 45(3). https://doi.org/10.1002/joc.8730

Song, Chunxiao, Xiao Huang, Oxley Les, Hengyun Ma, and Ruifeng Liu. 2022. *The Economic Impact of Climate Change on Wheat and Maize Yields in the North China Plain*. Vol. 19. MDPI.

Vanella, Daniela, Giuseppe Longo-Minnolo, Oscar Rosario Belfiore, Juan Miguel Ramírez-Cuesta, Salvatore Pappalardo, Simona Consoli, Guido D'Urso, Giovanni Battista Chirico, Antonio Coppola, and Alessandro Comegna. 2022. *Comparing the Use of ERA5 Reanalysis Dataset and Ground-Based Agrometeorological Data under Different Climates and Topography in Italy*. Vol. 42. Elsevier.

Wang, Xiaowen, Liang Li, Yibo Ding, Jiatun Xu, Yunfei Wang, Yan Zhu, Xiaoyun Wang, and Huanjie Cai. 2021. *Adaptation of Winter Wheat Varieties and Irrigation Patterns under Future Climate Change Conditions in Northern China*. Vol. 243. Elsevier.

Yassen, Ahmed Nagy, Won-Ho Nam, and Eun-Mi Hong. 2020. *Impact of Climate Change on Reference Evapotranspiration in Egypt*. Vol. 194. Elsevier.

Zolfaghari, Ali Asghar, Maryam Raeesi, Giuseppe Longo-Minnolo, Simona Consoli, and Miles Dyck. 2025. *Daily Reference Evapotranspiration Prediction in Iran: A Machine Learning Approach with ERA5-Land Data*. Vol. 59. Elsevier.